






Effect of dislocations on the performance of GaSb-based diode lasers grown on silicon

Cite as: J. Appl. Phys. **133**, 093103 (2023); doi: [10.1063/5.0135606](https://doi.org/10.1063/5.0135606)

Submitted: 21 November 2022 · Accepted: 11 February 2023 ·

Published Online: 2 March 2023



Andres Remis,  Laura Monge-Bartolomé,  Guilhem Boissier, Mounir Waguaf, Jean-Baptiste Rodriguez, 
Laurent Cerutti,  and Eric Tournié^{a)} 

AFFILIATIONS

IES, University of Montpellier, CNRS, F-34000 Montpellier, France

^{a)}Author to whom correspondence should be addressed: eric.tournie@umontpellier.fr

ABSTRACT

Silicon photonics is a promising technology for the fabrication of dense photonic chips, thanks to the very mature silicon industry. The direct epitaxial growth of III–V lasers on silicon is one of the main challenges for the realization of compact and robust mid-infrared sensors based on photonic integrated circuits. The crystal defects arising from this heteroepitaxial growth affect the laser performance and, therefore, need to be mitigated but also studied to better understand their impact on the laser operation. Here, we studied the effect of threading dislocations on laser performance by comparing the series of GaSb-based diode lasers grown on native GaSb and Si substrates with different numbers of quantum wells (n_{QW}) in their active zones. As expected, the laser threshold currents are higher in the case of diode lasers on Si, and they rapidly vary with n_{QW} . Still, the lowest threshold current densities are achieved with $n_{QW} = 1$ for both substrates. With the help of a theoretical gain model, we attribute these results to the fact that dislocations create non-radiative recombination but do not introduce additional optical losses. This work allows a better understanding of the origin of performance degradation and the decision to be made regarding the heterostructure design.

Published under an exclusive license by AIP Publishing. <https://doi.org/10.1063/5.0135606>

I. INTRODUCTION

The 2–5 μm mid-infrared (mid-IR) wavelength range presents transparency windows of the atmosphere as well as absorption lines of many biological and chemical species.¹ The demand for compact sensors in this wavelength range has increased significantly over the last decade for medical, industrial, and environmental applications. For now, these sensors are bulky and expensive because they are still composed of discrete devices. Silicon photonics offers the opportunity to reduce cost and footprint by combining the benefits of III–V semiconductors with the very advanced silicon industry.^{2,3} The monolithic integration of III–V lasers on silicon appears as the most promising approach for large-scale and cost-effective production of such compact and robust sensors.^{4–7} In this context, GaSb-based diode lasers (DLs), which cover the whole 2–3 μm wavelength range^{8,9} and are perfectly adapted to mid-IR sensing,^{10,11} have been recently grown on silicon substrates and demonstrated successful operation.¹²

The direct epitaxy of III–Vs on Si, however, leads to a large density of crystal defects such as threading dislocations (TDs) and antiphase boundaries (APBs) caused by the lattice, thermal, and

polarity mismatches between III–V materials and silicon.¹³ Whereas APBs can be suppressed,^{14,15} dislocations are unavoidable, even though their threading density can be reduced through various growth strategies.¹⁶ It is well known that they dramatically affect laser performances by inducing non-radiative recombinations in the active zone, which increases the threshold current density at the expense of the device's lifetime.^{17–21} Still, other aspects remain unclear in the literature where it is often stated that dislocations introduce optical losses as well.^{18,20,22,23}

In this work, we compared two series of GaSb-based DLs with different numbers of quantum wells (n_{QW}) in their active zones. One series was grown on native GaSb substrates, whereas the other one was grown on Si substrates. Their performances were confronted to a theoretical model, which allowed to extract the impact of dislocations on the gain and losses in the laser structures.

II. LASER STRUCTURE, GROWTH, AND PROCESS

Two sets of four samples containing different numbers of QWs ($1 \leq n_{QW} \leq 4$) were grown by solid-source molecular-beam epitaxy (MBE) on GaSb and (001)-oriented Si substrates exhibiting

a residual miscut of $\sim 0.5^\circ$ toward [110]. Their active zones, designed to emit near $2.3\mu\text{m}$, are based on 9-nm-thick $\text{Ga}_{0.67}\text{In}_{0.33}\text{As}_{0.08}\text{Sb}_{0.88}$ QWs confined by $\text{Al}_{0.25}\text{Ga}_{0.75}\text{As}_{0.02}\text{Sb}_{0.98}$ barrier layers and are embedded within $\text{Al}_{0.25}\text{Ga}_{0.75}\text{As}_{0.02}\text{Sb}_{0.98}$ waveguides.⁸ Two *n*- and *p*-type $\text{Al}_{0.9}\text{Ga}_{0.1}\text{As}_{0.08}\text{Sb}_{0.92}$ layers ensure carrier and photon confinements in the active region. A highly doped, *p*-type GaSb contact layer was grown atop all structures. In the case of DLs grown on Si substrates, a 1- μm thick GaSb buffer layer was first grown to suppress APBs.¹⁶ A highly conductive $\text{InAs}_{0.92}\text{Sb}_{0.08}$ contact layer was then grown to enable a top-top contact configuration, which avoids driving the current through the highly defective Si/GaSb interface.²² Finally, an additional 1- μm -thick GaSb buffer layer was inserted between the InAsSb contact layer and the laser structure. The laser structure with two QWs grown on Si is shown in Fig. 1(a) as an example. The QWs have a lattice-mismatch of $\sim 1.5\%$ with respect to GaSb, whereas the $\text{Al}_x\text{Ga}_{1-x}\text{As}_y\text{Sb}_{1-y}$ layers are lattice matched onto GaSb.

The growth conditions, doping profiles, and band structure details of these structures can be found in Ref. 12. Atomic-force microscopy (AFM) images [Fig. 1(b)] confirm the absence of APBs emerging at the surface of the samples grown on Si, whereas an

upper bound of $9 \times 10^7 \text{ cm}^{-2}$ is estimated for the threading dislocation density (TDD).

Broad-area and narrow-ridge DLs of different cavity lengths were fabricated. The DL process starts with the laser ridge definition using standard UV photolithography and inductively coupled plasma etching. The etching was stopped just before reaching the active zone, to minimize current spreading as well as optical losses on the sidewalls.²⁴ In the case of DLs on Si, a second etching was made to reach the $\text{InAs}_{0.92}\text{Sb}_{0.08}$ layer, which serves as the *n*-contact layer. Si_3N_4 was then deposited by plasma-enhanced chemical vapor deposition (PECVD) for electrical insulation and sidewall protection. The metallization was then carried out by the electron beam evaporation of Ti/Au on the top GaSb *p*-type layer and the $\text{InAs}_{0.92}\text{Sb}_{0.08}$ *n*-type layer in the case of DLs on Si. In the case of DLs grown on GaSb, Ti/Au was deposited on the top GaSb *p*-type layer and Pd/AuGeNi on the backside of the GaSb substrate that acts as the *n* contact. For both series, the substrates were thinned down by mechanical polishing to ease the cleavage of laser bars and no special treatment has been done to improve the reflectivity of the cleaved facets. The laser bars were then soldered on Cu heat sinks and measured on a probe station.

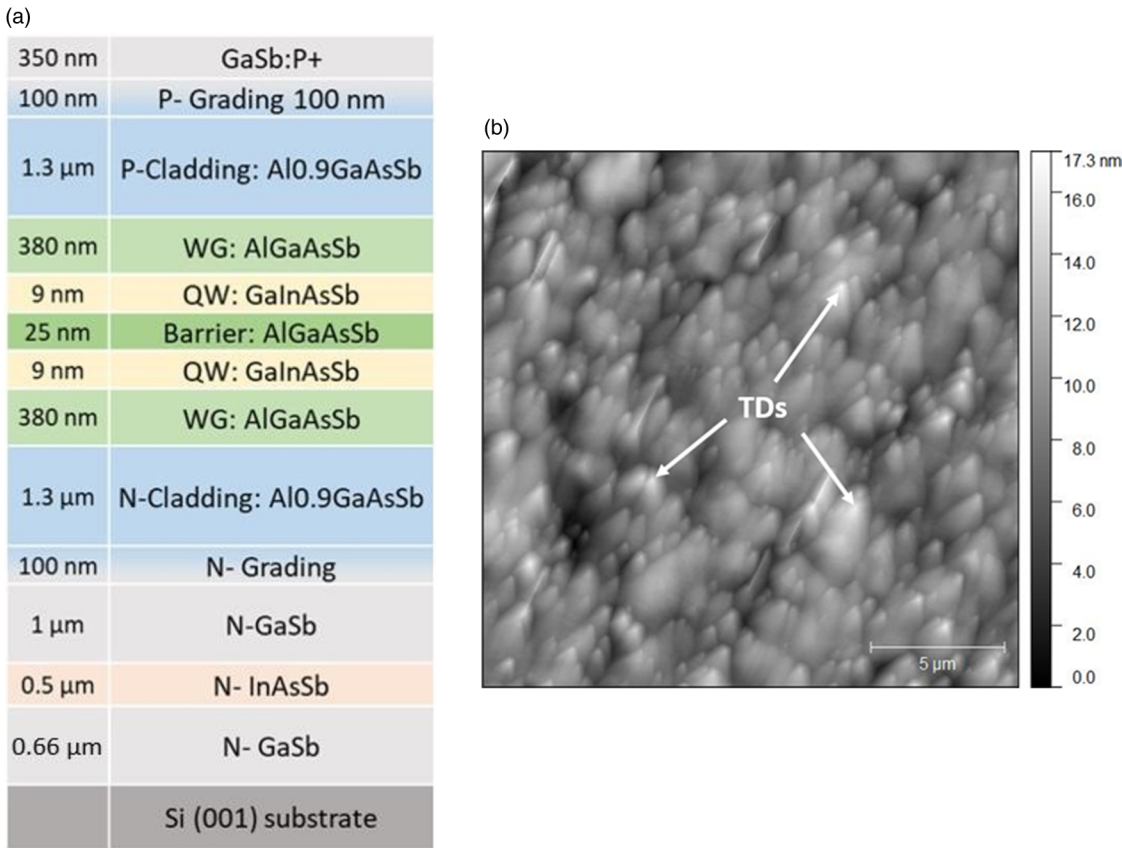


FIG. 1. (a) Design of the 2-QWs laser heterostructure grown on Si. (b) AFM image of the surface of the same laser.

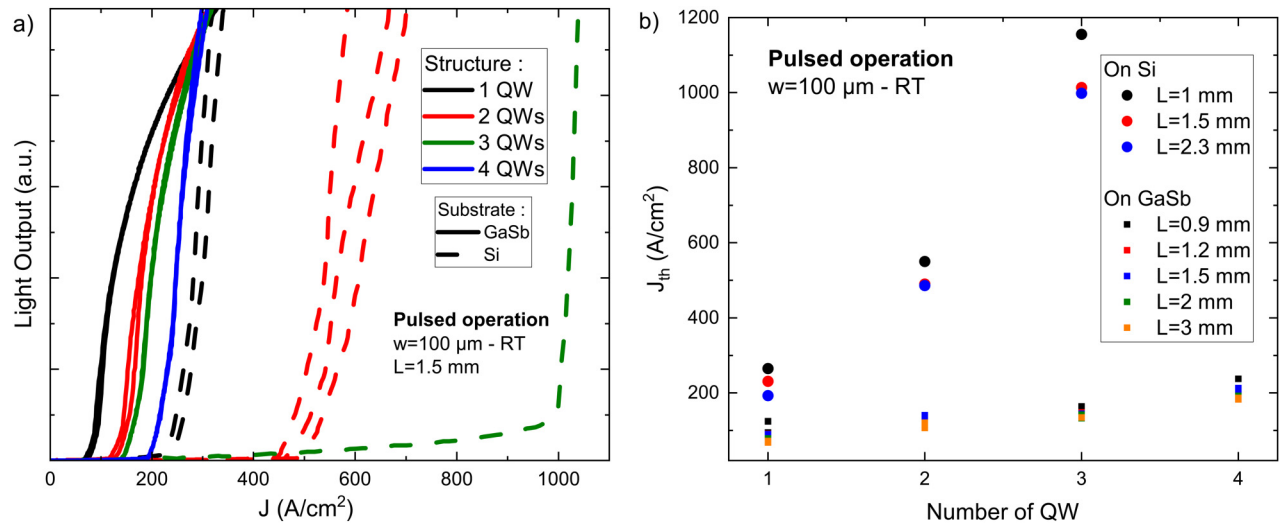


FIG. 2. Broad-area laser characteristics in pulsed operation for the two series. (a) Light output vs current density curves of 1.5 mm-long DLs with different numbers of QW. (b) Threshold current density vs the number of QWs for different cavity lengths.

III. LASER PROPERTIES

Broad-area DLs ($w=100\text{ }\mu\text{m}$) were first characterized in pulsed operation at room temperature (RT) to assess the threshold current density of the structure. As an example, the light output vs current (L-I) curves of the 1.5-mm long DLs with different QW numbers are plotted in Fig. 2(a) for the two series. To get an overview of the whole set of results, Fig. 2(b) shows the evolution of the threshold current density as a function of the QW number, for the different cavity lengths. DLs grown on native GaSb substrates exhibit lower threshold current densities than DLs grown on Si, as expected. For both series, the threshold current density increases with the QW number for every cavity length; therefore, the best threshold is obtained with the structures having one QW, whatever the substrate. However, the slope of $J_{th} = f(n_{QW})$ is much steeper for DLs grown on Si than for those grown on GaSb. As a consequence, we could not reach the threshold current with the DLs fabricated from the 4-QWs-structure grown on Si. Indeed, the extrapolated threshold would be $\sim 2.3\text{ kA/cm}^2$, which is beyond the limit of our setup. In contrast, the threshold current density (200 A cm^{-2}) obtained with the 1-QW structure is the best reported so far for GaSb-based DLs grown on Si.¹²

Narrow-ridge DLs were then measured in continuous wave (CW) at RT. The L-I-V data for 1-QW DLs grown on Si with an $8\text{-}\mu\text{m}$ wide ridge and different cavity lengths are plotted in Fig. 3(a). The turn-on voltage is in the 0.7–1 V range and the series resistance is around $4\text{ }\Omega$, comparable to that measured with DLs on GaSb substrates. The threshold currents range between 75 and 120 mA for cavity lengths between 1 and 2.3 mm, which are again the best results ever reported with GaSb-based DLs grown on Si.¹² The evolution of the slope efficiency ($\Delta P/\Delta I$) with the cavity length allows calculating the external quantum efficiency (η_d), and, in turn, the evolution with the cavity length of $1/\eta_d$ allows extracting

the internal losses α_i and the internal quantum efficiency η_i using the following equation:

$$\frac{1}{\eta_d} = \frac{1}{\eta_i} + \frac{\alpha_i}{\eta_i \ln(R^{-1})} L. \quad (1)$$

The internal losses for DLs on Si and on GaSb are plotted in Fig. 3(b). The results and the trends are similar for both series. The internal losses increase with the number of QWs, which we ascribe to increasing free carrier absorption and inhomogeneous carrier injection in the multi-QW structures.²⁵ In contrast, the internal quantum efficiency (not shown) remains constant at around $\sim 50\%$ for all structures.

Narrow-ridge DLs were also measured as a function of the temperature in CW. As an example, the L-I data for 2-QWs DLs grown on GaSb and Si, with a $10\text{-}\mu\text{m}$ wide ridge and a 1-mm long cavity is plotted in Fig. 4 for measurement temperatures from 20 to 70 °C (limited by the experimental setup). The threshold current varies between 42 and 82 mA for DLs on GaSb and between 120 and 200 mA for DLs on Si. The external quantum efficiency, which is proportional to the slope $\frac{\Delta P}{\Delta I}$, is lower for DLs grown on Si. Through the equations $I_{th}(T) = I_0 \exp\left(\frac{T}{T_0}\right)$ and $\eta_d = \eta_0 \exp\left(\frac{-T}{T_1}\right)$, we deduced the so-called characteristic temperatures T_0 and T_1 , which represent the sensitivity to the temperature of the laser threshold current and the external quantum efficiency, respectively. T_0 is similar on both substrates (91 and 97 K), whereas T_1 is lower for DLs on Si (117 K vs 147 K). Similar trends have been observed for all QW numbers. The lower T_1 for DLs on Si than on GaSb reflects the fact that the external quantum efficiency is sensitive to temperature due to the high TDD.

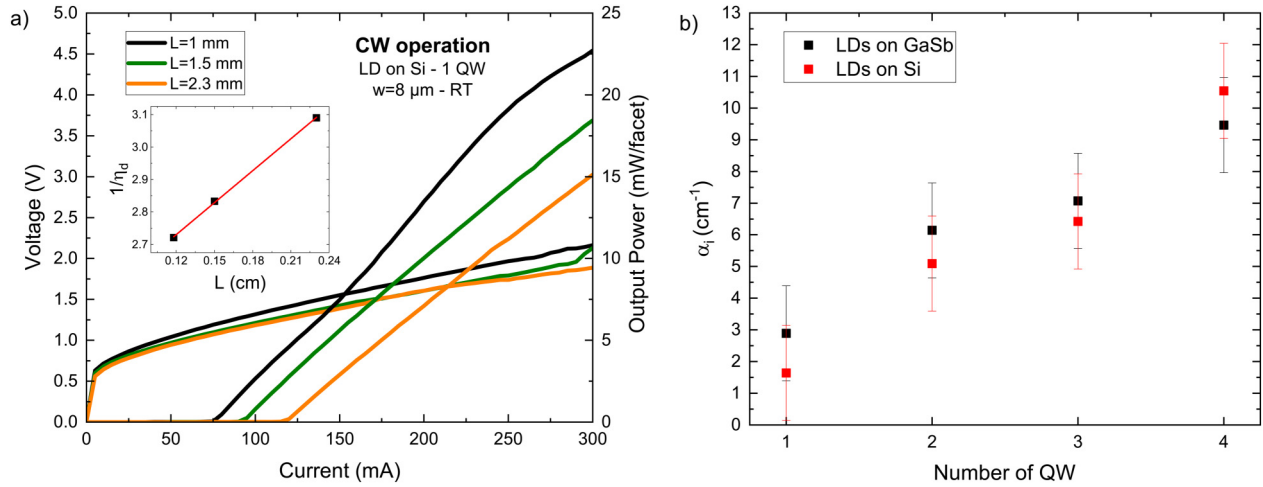


FIG. 3. Narrow-ridge laser characteristics in CW operation. (a) L–I–V data for 1 QW DLs grown on Si with an 8 μm-wide ridge and different cavity lengths. The inset shows the evolution of the reciprocal differential quantum efficiency. (b) Extracted internal losses vs the number of QWs for the two series.

IV. THEORETICAL GAIN MODEL

To analyze these experimental results and to understand the impact of the growth on Si, we modeled the properties of the structures. The threshold current density J_{th} is expressed as a function of the optical losses,^{26,27}

$$J_{th} = J_{tr} \exp\left(\frac{\alpha_i + \alpha_{FP}}{N_w \Gamma_w G_0}\right), \quad (2)$$

where N_w is the QW number, Γ_w is the overlap of the mode with the QWs ($\Gamma_w = 0.015$),^{27,28} G_0 is the gain parameter, J_{tr} is the transparency current density, α_i are the intrinsic internal losses, and α_{FP} are the Fabry–Pérot cavity losses, which is given as

$$\alpha_{FP} = \frac{1}{L} \ln(R^{-1}), \quad (3)$$

where R is the reflectivity of the facets at each end of the Fabry–Pérot cavity ($R \sim 0.3$)²⁷ of length L .

Besides the internal losses, J_{tr} and G_0 are needed to calculate the threshold current density from Eq. (2). They can be deduced from the optical gain of a single QW structure, which is calculated as a function of the energy of the emitted photon E and the carrier density N , thanks to the following equation:^{29,28,30,31}

$$g(E, N) = \frac{\pi e^2 \hbar M_l^2}{\epsilon_0 n c m_0 E} \rho(E) (f_c(E, N) - f_v(E, N)), \quad (4)$$

where $\rho(E)$ is the density of states, $f_c(E, N)$ and $f_v(E, N)$ are the Fermi functions in the conduction band and in the valence band, respectively, M_l is the dipole matrix element, and n is the real part of the refractive index. The gain broadening caused by the intra-band scattering is taken into account in the model by convoluting the calculated gain by a Lorentzian function (5),^{28,31}

$$L(E) = \frac{1}{\pi} \frac{\frac{\hbar}{\tau_{in}}}{\left(\frac{\hbar}{\tau_{in}}\right)^2 + E^2}, \quad (5)$$

where τ_{in} is the intersubband relaxation time.

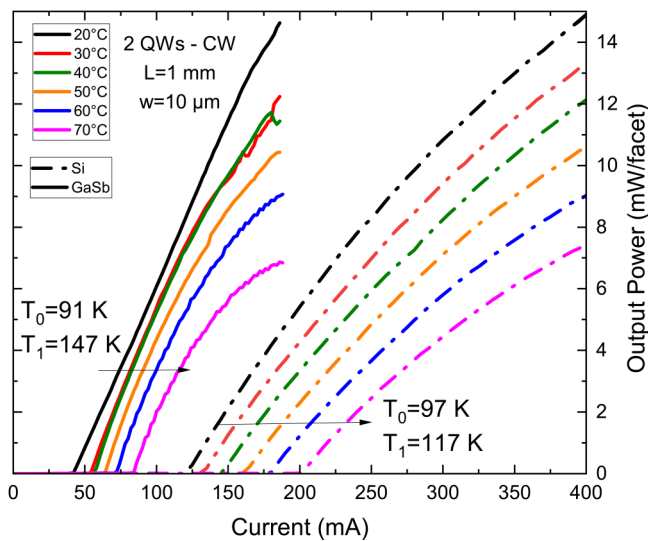


FIG. 4. L–I data for 2-QWs DLs on Si and GaSb with a 10-μm wide ridge and 1-mm long cavity for different measurement temperatures.

The modal gain is then obtained using the following expression:^{28,31}

$$G_{\text{modal}}(E, N) = N_W \Gamma_W G_{\text{conv}}(E, N), \quad (6)$$

where $G_{\text{conv}}(E, N)$ is the gain convoluted with the Lorentzian function.

Afterward, we calculated the modal gain at the energy of the peak modal gain. Finally, we calculated the modal gain as a function of the current density $G_{\text{modal}}(J)$ by substituting N by J , thanks to the following equation:

$$J = \frac{qN_W L_W}{\eta_i} (AN + BN^2 + CN^3), \quad (7)$$

where L_W is the QW width; η_i is the internal quantum efficiency taken from the experimental results; and A , B , and C are the SRH (Shockley–Read–Hall), radiative, and Auger recombination coefficients, respectively.⁸

The modal gain as a function of the current density $G_{\text{modal}}(J)$ is now known, and the parameters J_{tr} and G_0 can, finally, be extracted using the following equation, as well as the threshold current density seen above [Eq. (2)]:

$$G_{\text{modal}}(J) = N_W \Gamma_W G_0 \ln\left(\frac{J}{J_{\text{tr}}}\right). \quad (8)$$

We fitted these J_{th} values to the experimental values for both series of DLs on GaSb and DLs on Si, by adjusting the SRH coefficient A , while coefficients B and C were taken from the literature.^{27,28} We used the same B and C coefficients for both substrates since they are intrinsic to the materials and heterostructures.

Figure 5 shows the experimental and fitted J_{th} values for the two series. The agreement for the DLs grown on GaSb is excellent. In contrast, for the DLs grown on Si it was not possible to adjust all experimental curves assuming the same A SRH coefficient (Fig. 5), which suggests that for these DLs, the A coefficient increases with the number of QWs. We tentatively ascribe this behavior to the introduction of two new QW/barrier interfaces for every additional QW in the structure. In turn, at such high dislocation densities, misfit dislocation arms propagate at each interface and create additional non-radiative recombinations,^{32–34} which is also consistent with the steep variation in the threshold current density with the number of QWs observed for the DLs grown on Si [Fig. 2(b)].

The final values used to fit all data are in Table I. For the A coefficient, the final values for the DLs grown on GaSb are close to those found in the literature,^{27,28} whereas much higher values have to be used for the DLs grown on Si to account for non-radiative SRH recombination introduced by the dislocations.³⁵

Finally, we show in Fig. 6(a) the calculated modal gain vs current density curves for all DLs grown on both GaSb and Si substrates. First, we observed that the transparency current density J_{tr} (J for which the modal gain equals zero) increases with the QW number, as expected. Above transparency, the differential modal gain increases with the number of QWs.³⁶ For the DLs grown on Si, the larger SRH recombinations increase the transparency

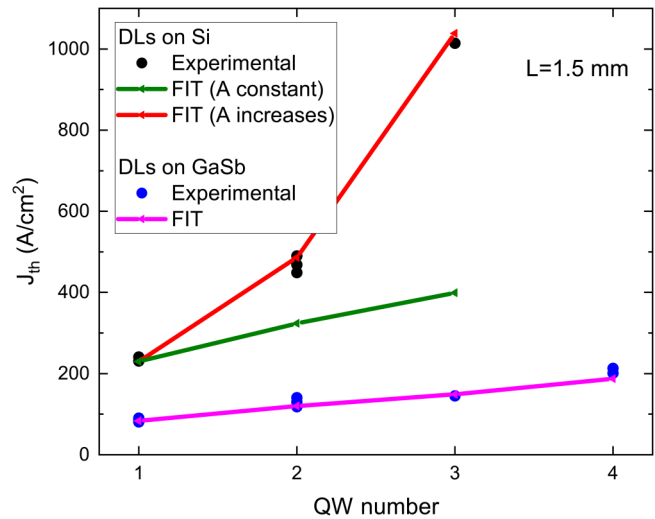


FIG. 5. Fits of the threshold current density for the two series for the 1.5-mm long DLs.

current and all curves are shifted toward larger current densities, whereas the modal gain decreases. This results in an increased laser threshold [Eq. (2)], as also observed experimentally [Fig. 2(b)].

Figure 6(a) can be used to determine the optimal number of QWs if the total losses are known. The total losses of DLs grown on native GaSb substrates have typically been measured by different groups in the 10–20 cm^{-1} range.^{9,26,28} If we consider total losses of 10 cm^{-1} , for example, the modal gain equals this value at the laser threshold. The lowest threshold current density is then obtained for a structure having one QW [Fig. 6(a)]. In contrast, for total losses of 15 cm^{-1} , the lowest threshold current density is obtained for a structure with two QWs [Fig. 6(a)]. Thus, when the optical losses increase, the optimal QW number switches from one to two QWs at 12.2 cm^{-1} in the case of DLs on GaSb and at 14 cm^{-1} in the case of DLs on Si, as it is summarized in Fig. 6(b). The fact that these values are very similar (12.2 and 14 cm^{-1}), and that the optimal QW number for both DLs on Si and on GaSb is the same (one QW), indicates that threading dislocations do not introduce significant optical losses to the structures, in contrast to what is often claim. It confirms also the results shown in Fig. 3(b) where the extracted internal losses for both DLs on Si and on GaSb are very similar.

TABLE I. Recombination coefficient values.

Coefficient	DLs on GaSb		DLs on Si	
	1–4 QWs	1 QW	2 QWs	3 QWs
A (s^{-1})	3.9×10^7	1.1×10^8	1.3×10^8	2.4×10^8
B ($\text{cm}^3 \text{s}^{-1}$)	4.4×10^{-10}	4.4×10^{-10}	4.4×10^{-10}	4.4×10^{-10}
C ($\text{cm}^6 \text{s}^{-1}$)	2×10^{-28}	2×10^{-28}	2×10^{-28}	2×10^{-28}

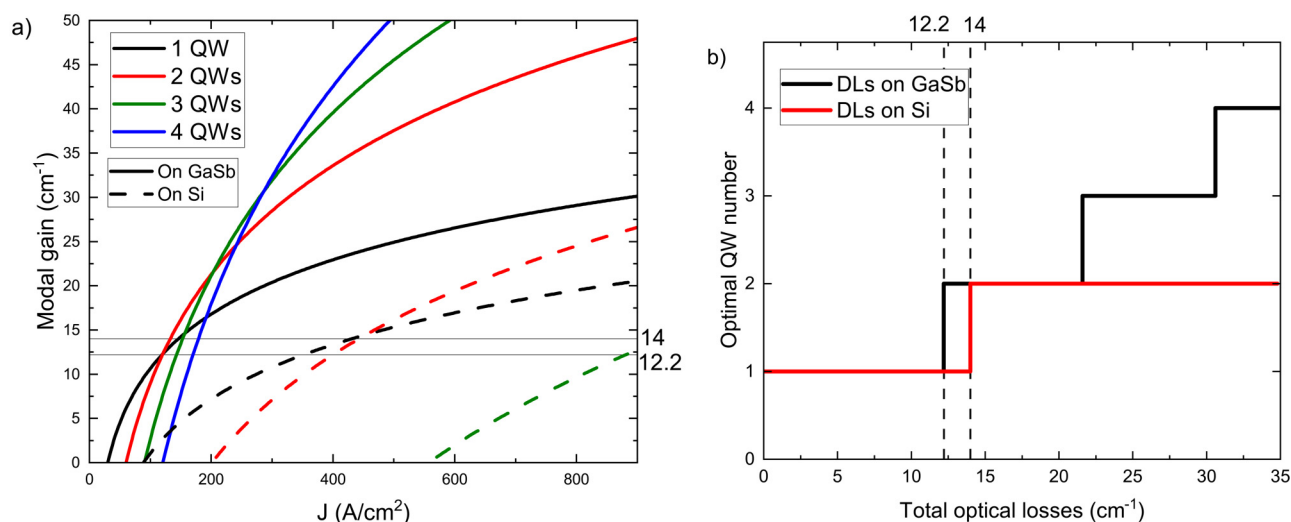


FIG. 6. The gain model calculations for the two series. (a) Modal gain vs current density curves for different number of QWs. (b) The optimal number of QWs vs the total optical losses.

V. CONCLUSIONS

To conclude, we fabricated and characterized two series of GaSb-based DLs grown on GaSb and Si substrates and containing different numbers of QWs in their active zone. We have studied and analyzed the effect of threading dislocations on the performance of DLs on Si by comparing with DLs grown on GaSb. DLs on Si exhibit, as expected, higher thresholds than DLs grown on GaSb even though the optimum number of QWs is the same in both cases (one QW). The theoretical model used in this work allowed us to understand the gain properties of these structures and to demonstrate that the performance degradation on Si arises from increased SRH recombinations, without additional optical losses. We have also shown that the SRH recombination coefficient of the DLs grown on Si increases with the number of QWs. This work allows a better understanding of performance degradation, which is important for the decision making regarding the heterostructure design. This allowed us to demonstrate record threshold currents for GaSb DLs grown on Si thanks to a single QW heterostructure.

ACKNOWLEDGMENTS

Part of the work was supported by the French ANR (LightUp, No. ANR-19-CE24-0002) and by the French Program on “Investments for the Future” (Equipex EXTRA, No. ANR-11-EQPX-0016).

AUTHOR DECLARATIONS

Conflict of Interest

The authors have no conflicts to disclose.

Author Contributions

Andres Remis: Conceptualization (equal); Formal analysis (equal); Investigation (equal); Methodology (equal); Software (equal); Writing – original draft (equal). **Laura Monge-Bartolomé:** Investigation (equal); Methodology (equal). **Guilhem Boissier:** Methodology (equal). **Mounir Waguaf:** Data curation (equal); Investigation (equal). **Jean-Baptiste Rodriguez:** Conceptualization (equal); Investigation (equal); Methodology (equal); Validation (equal); Writing – review & editing (equal). **Laurent Cerutti:** Conceptualization (equal); Investigation (equal); Methodology (equal); Validation (equal). **Eric Tournié:** Conceptualization (equal); Investigation (equal); Methodology (equal); Supervision (equal); Validation (equal); Writing – review & editing (equal).

DATA AVAILABILITY

The data that support the findings of this study are available within the article.

REFERENCES

1. E. Gordon, L. S. Rothman, R. J. Hargreaves, R. Hashemi, E. V. Karlovets, F. M. Skinner, E. K. Conway, C. Hill, R. V. Kochanov, Y. Tan, P. Wcislo, A. A. Finenko, K. Nelson, P. F. Bernath, M. Birk, V. Boudon, A. Campargue, K. V. Chance, A. Coustenis, B. J. Drouin, J.-M. Flaud, R. R. Gamache, J. T. Hodges, D. Jacquemart, E. J. Mlawer, A. V. Nikitin, V. I. Perevalov, M. Rotger, J. Tennyson, G. C. Toon, H. Tran, V. G. Tyuterev, E. M. Adkins, A. Baker, A. Barbe, E. Cané, A. G. Császár, A. Dudaryonok, O. Egorov, A. J. Fleisher, H. Fleurbaey, A. Foltynowicz, T. Furtenbacher, J. J. Harrison, J.-M. Hartmann, V.-M. Horneman, X. Huang, T. Karman, J. Karns, S. Kass, I. Kleiner, V. Kofman, F. Kwabia-Tchana, N. N. Lavrentieva, T. J. Lee, D. A. Long, A. A. Lukashvskaya, O. M. Lyulin, V. Y. Makhnev, W. Matt, S. T. Massie, M. Melosso, S. N. Mikhailenko, D. Mondelain, H. S. P. Müller, O. V. Naumenko, A. Perrin, O. L. Polyansky, E. Raddaoui, P. L. Raston,

- Z. D. Reed, M. Rey, C. Richard, R. Tóbiás, I. Sadiek, D. W. Schwenke, E. Starikova, K. Sung, F. Tamassia, S. A. Tashkun, J. Vander Auwera, I. A. Vasilenko, A. A. Vigin, G. L. Villanueva, B. Vispoel, G. Wagner, A. Yachmenev, and S. N. Yurchenko, *J. Quant. Spectrosc. Radiat. Transf.* **277**, 107949 (2022).
- ²R. Soref, *Nat. Photonics* **4**, 495 (2010).
- ³S. Y. Siew, B. Li, F. Gao, H. Y. Zheng, W. Zhang, P. Guo, S. W. Xie, A. Song, B. Dong, L. W. Luo, C. Li, X. Luo, and G.-Q. Lo, *J. Lightwave Technol.* **39**, 4374 (2021).
- ⁴A. Y. Liu and J. Bowers, *IEEE J. Sel. Top. Quantum Electron.* **24**(6), 6000412 (2018).
- ⁵Z. Zhou, B. Yin, and J. Michel, *Light Sci. Appl.* **4**, e358 (2015).
- ⁶M. Tang, J.-S. Park, Z. Wang, S. Chen, P. Jurczak, A. Seeds, and H. Liu, *Prog. Quantum Electron.* **66**, 1 (2019).
- ⁷N. Margalit, C. Xiang, S. M. Bowers, A. Bjorlin, R. Blum, and J. E. Bowers, *Appl. Phys. Lett.* **118**, 220501 (2021).
- ⁸E. Tournié and L. Cerutti, in *Mid-Infrared Optoelectronics Materials, Devices, and Applications* (Woodhead Publishing, Duxford, 2020).
- ⁹G. Belenky and L. Shterengas, in *Semiconductor Lasers: Fundamentals and Applications*, edited by A. Baranov and E. Tournié (Woodhead Publishing, 2013), p. 441, ISBN: 9780857091215.
- ¹⁰T. Bleuel, M. Brockhaus, J. Koeth, J. Hofmann, R. Werner, and A. W. B. Forchel, "GaInAsSb/AlGaAsSb: single-mode DFB lasers for gas sensing in the 2- μ m wavelength range," in *Proc. SPIE 3858, Advanced Materials and Optical Systems for Chemical and Biological Detection*, edited by M. Fallahi and B. I. Swanson (SPIE, 1999), p. 119.
- ¹¹K. Vizbaras, E. Dvinelis, I. Šimonytė, A. Trinkūnas, M. Greibus, R. Songaila, T. Žukauskas, M. Kaušylas, and A. Vizbaras, *Appl. Phys. Lett.* **107**, 011103 (2015).
- ¹²M. Rio Calvo, L. Monge Bartolomé, M. Bahriz, G. Boissier, L. Cerutti, J.-B. Rodriguez, and E. Tournié, *Optica* **7**, 263 (2020).
- ¹³H. Kroemer, *J. Cryst. Growth* **81**, 193 (1987).
- ¹⁴C. Cornet, S. Charbonnier, I. Lucci, L. Chen, A. Létoublon, A. Alvarez, K. Tavernier, T. Rohel, R. Bernard, J.-B. Rodriguez, L. Cerutti, E. Tournié, Y. Léger, M. Bahri, G. Patriarche, L. Largeau, A. Ponchet, P. Turban, and N. Bertru, *Phys. Rev. Mater.* **4**, 053401 (2020).
- ¹⁵M. Rio Calvo, J.-B. Rodriguez, C. Cornet, L. Cerutti, M. Ramonda, A. Trampert, G. Patriarche, and E. Tournié, *Adv. Electron. Mater.* **8**, 2100777 (2022).
- ¹⁶M. Rio Calvo, "GaSb epitaxy on Si for integrated optoelectronics," Ph.D. thesis (University of Montpellier, 2020).
- ¹⁷A. Y. Liu, R. W. Herrick, O. Ueda, P. M. Petroff, A. C. Gossard, and J. E. Bowers, *IEEE J. Sel. Top. Quantum Electron.* **21**, 690 (2015).
- ¹⁸J. Liu, M. Tang, H. Deng, S. Shutts, L. Wang, P. M. Smowton, C. Jin, S. Chen, A. Seeds, and H. Liu, *J. Phys. D: Appl. Phys.* **55**, 404006 (2022).
- ¹⁹C. Hantschmann, Z. Liu, M. Tang, S. Chen, A. J. Seeds, H. Liu, I. H. White, and R. V. Penty, *J. Lightwave Technol.* **38**, 4801 (2020).
- ²⁰Z. Liu, M. Martin, T. Baron, S. Chen, A. Seeds, R. Penty, I. White, H. Liu, C. Hantschmann, M. Tang, Y. Lu, J.-S. Park, M. Liao, S. Pan, A. Sanchez, and R. Beanland, *J. Lightwave Technol.* **38**, 240 (2020).
- ²¹J. Selvidge, J. Norman, M. E. Salmon, E. T. Hughes, J. E. Bowers, R. Herrick, and K. Mukherjee, *Appl. Phys. Lett.* **115**, 131102 (2019).
- ²²J. R. Reboul, L. Cerutti, J. B. Rodriguez, P. Grech, and E. Tournié, *Appl. Phys. Lett.* **99**, 121113 (2011).
- ²³J. R. Orchard, S. Shutts, A. Sobiesierski, J. Wu, M. Tang, S. Chen, Q. Jiang, S. Elliott, R. Beanland, H. Liu, P. M. Smowton, and D. J. Mowbray, *Opt. Express* **24**, 6196 (2016).
- ²⁴L. Monge Bartolomé, "Toward mid-infrared semiconductor lasers on silicon photonic integrated circuits," Ph.D. thesis (University of Montpellier, 2021).
- ²⁵M. Rattunde, J. Schmitz, R. Kiefer, and J. Wagner, *Appl. Phys. Lett.* **84**, 4750 (2004).
- ²⁶Y. Rouillard, J. Angellier, A. Salhi, P. Grech, and F. Chevrier, "GaInAsSb/AlGaAsSb laser diodes for the 2- to 3- μ m range," in *Proceedings of SPIE - The International Society for Optical Engineering 5738*, edited by C. Mermelstein and D. P. Bour (SPIE, 2005), p. 120.
- ²⁷Y. Rouillard, "Diodes laser GaInAsSb/AlGaAsSb pour émission dans la gamme 2-3 μ m et au-delà," Micro et nanotechnologies/Microélectronique. Université de Montpellier 2 (2007).
- ²⁸A. Salhi and A. A. Al-Muhanna, *IEEE J. Sel. Top. Quantum Electron.* **15**, 918 (2009).
- ²⁹T. Makino, *IEEE J. Quantum Electron.* **32**, 493 (1996).
- ³⁰S. Belahsene, *Innovative Mid-Infrared Lasers for Hydrocarbon Analysis* (University of Montpellier, 2011).
- ³¹L. A. Coldren and S. W. Corzine, *Diode Lasers and Photonic Integrated Circuits*, Wiley Series in Microwave and Optical Engineering, edited by K. Chang (Wiley, 1995).
- ³²M. E. Groenert, C. W. Leitz, A. J. Pitera, V. Yang, H. Lee, R. J. Ram, and E. A. Fitzgerald, *J. Appl. Phys.* **93**, 362 (2003).
- ³³M. E. Groenert, A. J. Pitera, R. J. Ram, and E. A. Fitzgerald, *J. Vac. Sci. Technol. B* **21**, 1064 (2003).
- ³⁴J. Selvidge, J. Norman, E. T. Hughes, C. Shang, D. Jung, A. A. Taylor, M. J. Kennedy, R. Herrick, J. E. Bowers, and K. Mukherjee, *Appl. Phys. Lett.* **117**, 122101 (2020).
- ³⁵A. Alkauskas, C. E. Dreyer, J. L. Lyons, and C. G. Van de Walle, *Phys. Rev. B* **93**, 201304 (2016).
- ³⁶L. Shterengas, G. Belenky, G. Kipshidze, and T. Hosoda, *Appl. Phys. Lett.* **92**, 171111 (2008).